Development of an Anelastic Vector Vorticity Model on the Icosahedral Geodesic Grid

Ross Heikes, C.S. Konor, Joon-Hee Jung and D. Randall

Dept. of Atmospheric Science
Colorado State University

Outline

1. Describe the icosahedral grid
   - parallel domain decomposition
   - parallel communication
2. Describe the 2D Poisson solver and show scaling results several computer platforms.
3. Describe the current anelastic model and resulting 3D Poisson solver
4. Show results for the 3D solver.

Icosahedral grid basics

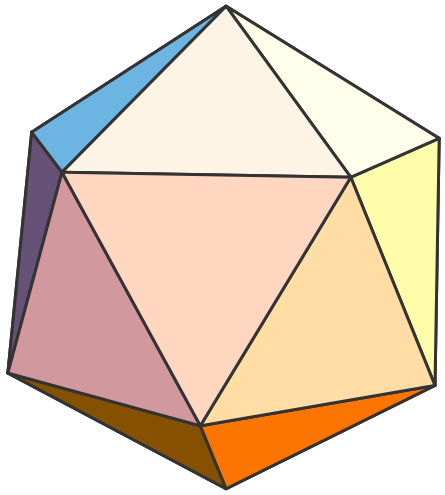

Consider
the icosahedron

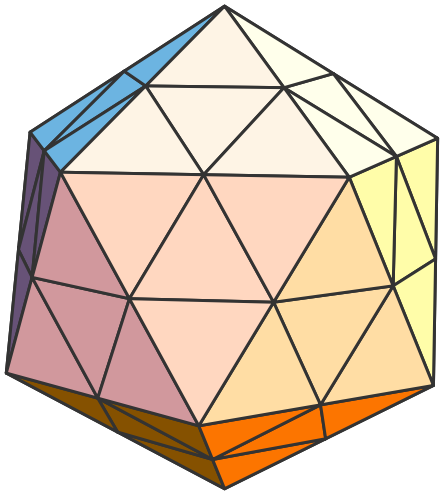

Bisect each edge
to form new faces

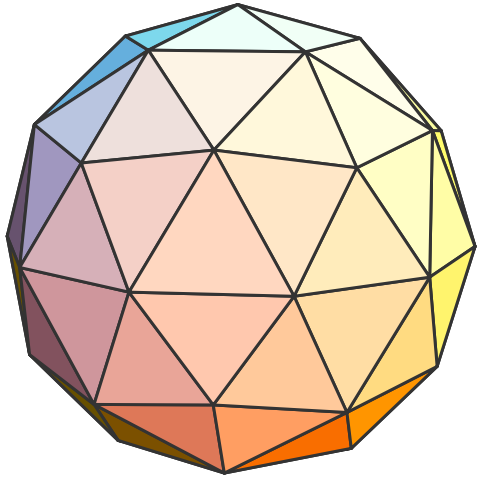

Project new vertices

- The vertices are the model grid points.
- Numerous algorithms exist to adjust grid point positions to optimize grid properties.
- Each grid point on a coarser resolution can be associated with four grid points after the bisection.

Voronoi cells

- An area is associated with each vertex. These areas are the control volumes of the finite-difference operators. These areas are Voronoi cells.

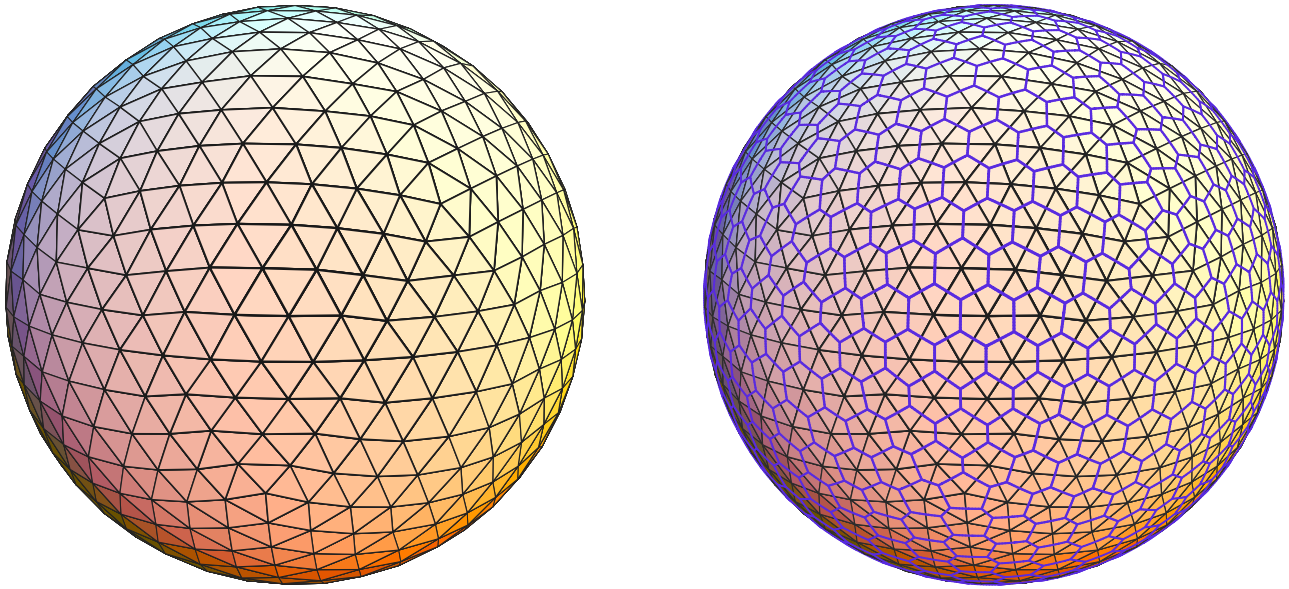

- There are 12 pentagons (associated with the vertices of the original icosahedron) and N-12 hexagonal cells.
- This grid provides approximately homogeneous and isotropic resolution over the sphere.

Counting the cells

✦ The global number of grid points is given by

$$N = 2 + 10 \times 2^{2r}$$

where r is the number of applications of the subdivision algorithm.

resolution (r)	number of cells	global grid point spacing (km)
9	2,621,442	15.64
10	10,485,762	7.819
11	41,943,042	3.909
12	167,772,162	1.955
13	671,088,642	0.997

Parallel domain decomposition

- Concatenating the faces of the icosahedron allows the sphere to be partitioned into 10 quadrilateral regions (subdomains).

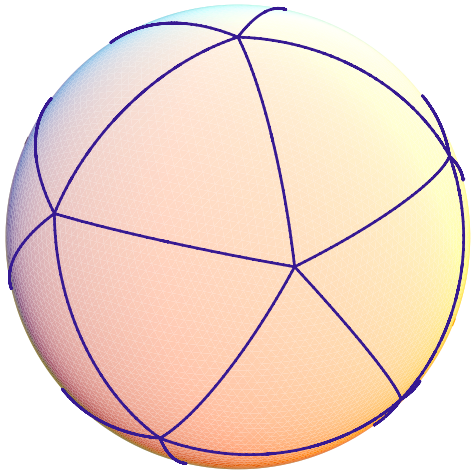

Icosahedron projected to sphere

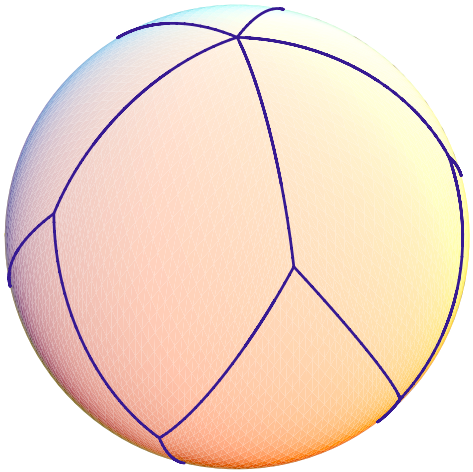

10 quadrilateral regions

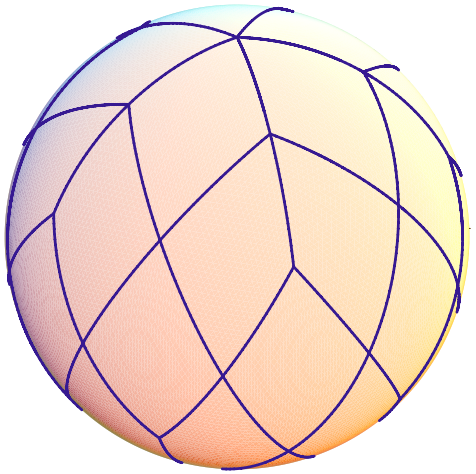

40 quadrilateral regions

- All the cells within a given subdomain are assigned to a process.
- Any subset of the global number of subdomain can be assigned to a process.

Parallel communication

- Ghost cell values are communicated between processes
- Nonblocking MPI (MPI_ISEND, MPI_IRECV and MPI_WAITALL) is used for communication between subdomain blocks.
- The processes can exchange arbitrarily wide ghost cell regions.
- There is an option to separate send/recv from wait to allow for overlap of communication and computation.

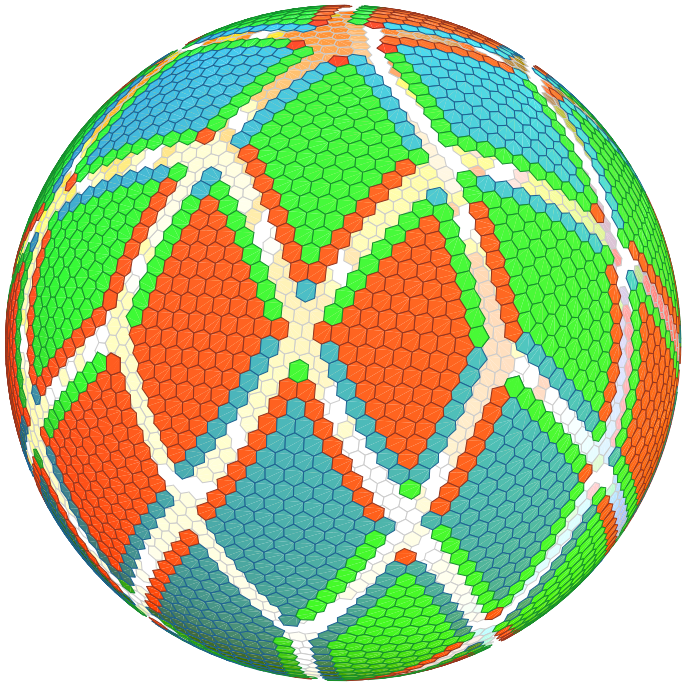

Assigning subdomains to processes

- Subdomains are numbered with a Morton-style ordering. The pattern for the numbering is recursively repeated.

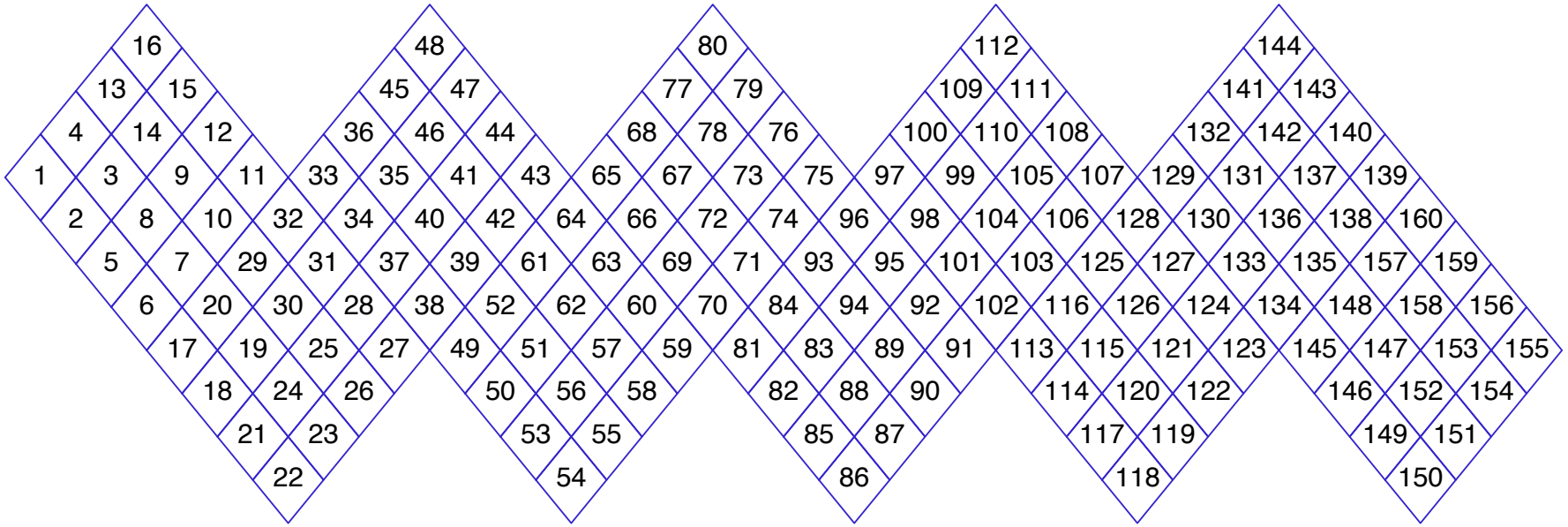

- Leverage the increasing number of cores SMP computer architectures:
  - OpenMP or shared memory (remote memory access) communication between physically close processes within a node
  - MPI message passing between nodes

Equations of the hydrostatic dynamical core

✦ Continuity

$$\frac{\partial m}{\partial t} + \nabla\cdot\left(m\mathbf{V}\right) + \frac{\partial}{\partial \zeta}\left(m\dot{\zeta}\right) = 0$$

✦ Thermodynamic

$$\frac{\partial \theta}{\partial t} + \mathbf{V}\cdot\nabla\theta + \dot{\zeta}\frac{\partial \theta}{\partial \zeta} = \frac{Q}{\Pi}$$

✦ Vorticity and Divergence

$$\frac{\partial \eta}{\partial t} + \nabla\cdot\left(\eta\mathbf{V}\right) + \mathbf{k}\cdot\left[\nabla\times\left(\dot{\zeta}\frac{\partial \mathbf{V}}{\partial \zeta}\right)\right] = J\left(\theta,\Pi\right) + \mathbf{k}\cdot\left[\nabla\times\mathbf{F}\right]$$

$$\frac{\partial \delta}{\partial t} + J(\eta,\chi) - \nabla\cdot\left(\eta\nabla\psi\right) + \nabla^2 K + \nabla\cdot\left(\dot{\zeta}\frac{\partial \mathbf{V}}{\partial \zeta}\right) = -\nabla^2 M + \nabla\cdot\left(\Pi\nabla\theta\right) + \nabla\cdot\mathbf{F}$$

✦ Elliptic Equations

$$\nabla^2\psi = \eta - f \quad \text{and} \quad \nabla^2\chi = \delta$$

Sample output

- Jablonowski and Williamson (2006)
  Quart. J. Roy. Meteor. Soc., **132,** 2943-2975
- 655362 cells (31.3km)
  on 640 cores
- 850hPa relative vorticity
  and surface temperature

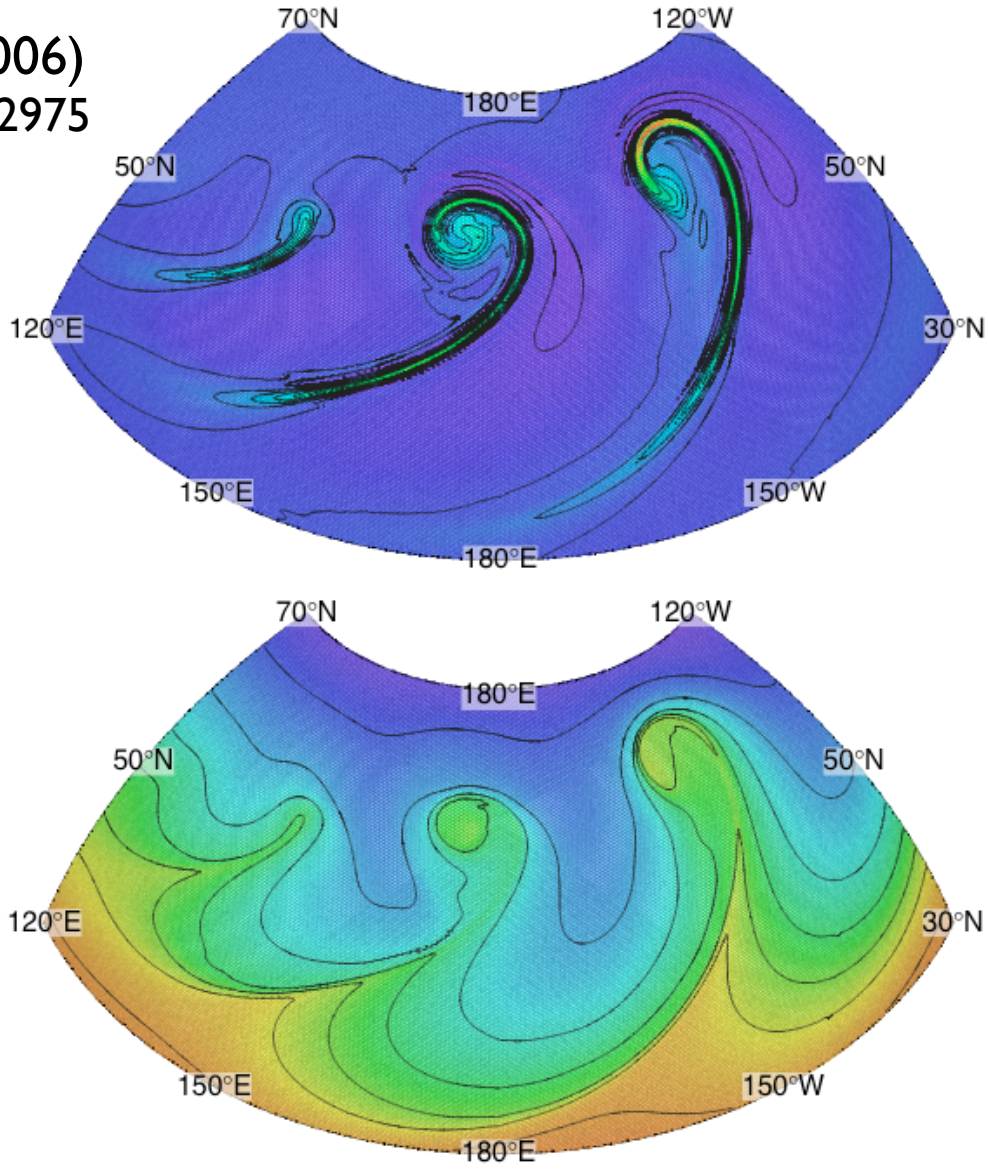

Multigrid on the icosahedral grid

- Several of our models require solving the Poisson equation:

$$\nabla^2 \alpha = \beta$$

- The grid's recursive structure facilitates use of multigrid methods.
- There are two main parts to the multigrid algorithm:

  1) Relaxation or smoothing operator

  2) Transferring information between grid resolutions:

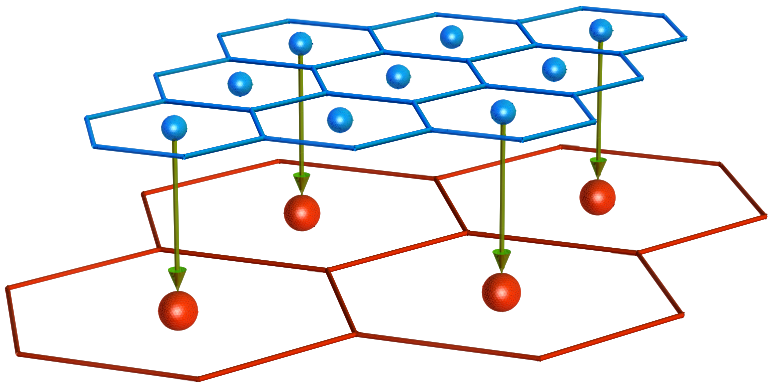

Restriction

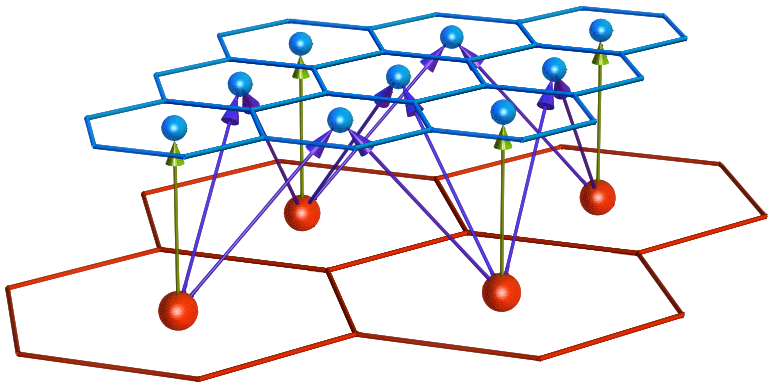

Prolongation

2D Poisson equation solver

- The continuous equation

$$\nabla^2 \alpha = \beta$$

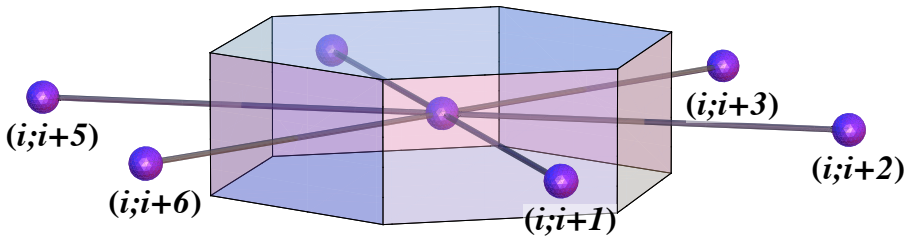

- The discrete equation

$$\frac{1}{A_i} \sum_{i'} \frac{\alpha_{i+i'}^{(\kappa)} - \alpha_i^{(\kappa+1)}}{L_{i;i+i'}} l_{i;i+i'} = \beta_i$$

where (κ) denotes an iteration index.

- Diagonalized system is re-arrange to form the relaxation operator

$$\alpha_i^{(\kappa+1)} = \left[\sum_{i'} \frac{l_{i;i+i'}}{L_{i;i+i'}} \right]^{-1} \left[A_i \beta_i - \sum_{i'} \frac{l_{i;i+i'}}{L_{i;i+i'}} \alpha_{i+i'}^{(\kappa)} \right]$$

Multigrid on the icosahedral grid

- As information is transfered to coarser grids the coarser subdomains contain fewer cells.
- It becomes necessary to deactivate processors
  - the number of cells is less than the number of processors
  - work per process becomes prohibitively small
- For example, consider a transfer between 160 subdomains and 40 subdomains

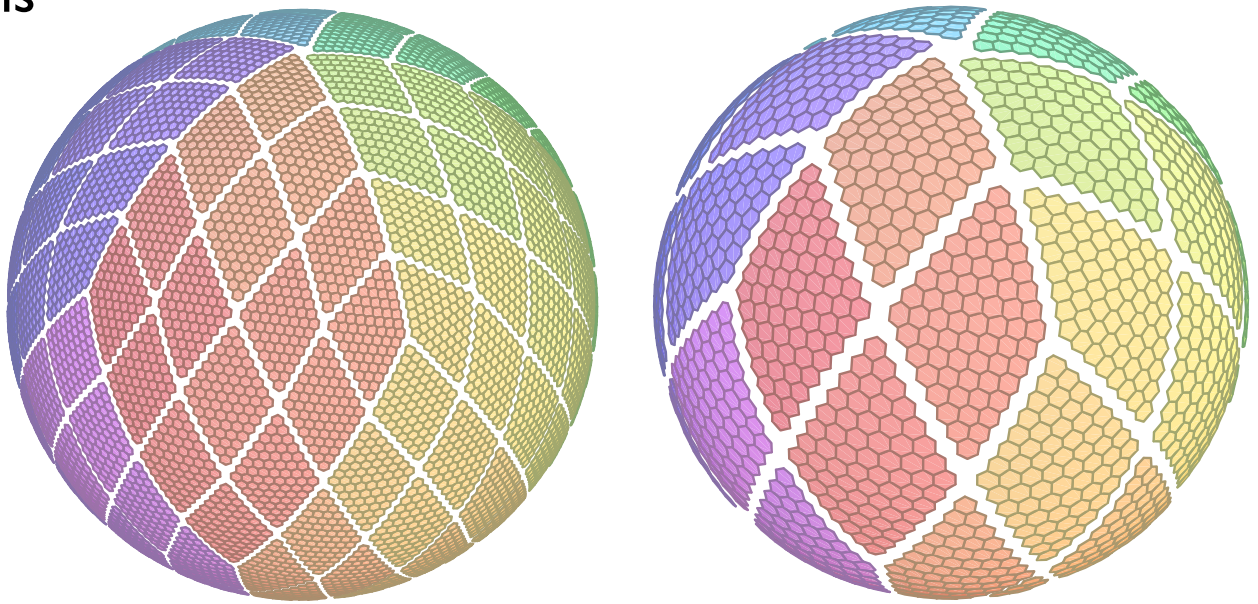

Franklin at NERSC

- Franklin at the National Energy Research Scientific Computing Center (NERSC). **Cray XT4** system with 9,660 compute nodes. Each node has dual processor cores, and the entire system has a total of **19,320 processor cores** of a 2.6 GHz dual-core AMD Opteron processors. Each compute node has 4 GBytes of memory.

Franklin (20 V-cycles, 20 layers)

Time (s)		Processes				
		640	1280	2560	5120	10240
Grid resolution	2621442 (9) (15.64km)	0.494	0.376	0.289	0.254	0.223
	10485762 (10) (7.819km)	1.793	1.042	0.521	0.400	
	41943042 (11) (3.909km)	6.668	3.281	1.798	0.859	0.532

Anelastic vector vorticity model on the icosahedral grid

- We are currently constructing and testing a Global Cloud Resolving Model (GCRM). This is under a DOE-SciDAC project.
- Based on Jung and Arakawa (2008, *MWR*, **136**, 276-294)
- The model ***Predicts 3D vorticity*** instead of momentum. In this formulation the 3D vorticity vector is guaranteed to be nondivergent.
- Elliptic equation is used to obtain vertical velocity *w* instead of nonhydrostatic pressure.
- This model will be modified to use the newly developed **unified system** of equations. This system of equations unifies the non-hydrostatic analestic and quasi-hydrostatic systems of equations.

Anelastic vector vorticity model prognostic equations

✦ Horizontal component of vorticity $\boldsymbol{\eta}$

$$\frac{\partial \tilde{\boldsymbol{\eta}}}{\partial t} = -\overbrace{\nabla_H \cdot \left(\tilde{\boldsymbol{\eta}}\mathbf{v}\right)}^{\text{horizontal advection}} - \overbrace{\frac{\partial}{\partial z}\left(\tilde{\boldsymbol{\eta}} w\right)}^{\text{vertical advection}} + \overbrace{\tilde{\boldsymbol{\eta}} \cdot \nabla_H \mathbf{v}}^{\text{stretching}} + \overbrace{\tilde{\xi}\frac{\partial \mathbf{v}}{\partial z}}^{\text{tilting}} + \mathbf{v}\nabla_H \cdot \left(2\boldsymbol{\Omega}_H\right) - \overbrace{\mathbf{k} \times \nabla_H B}^{\text{buoyancy}} + \overbrace{\mathbf{k} \times \left(\frac{\partial \mathbf{F}_\mathbf{v}}{\partial z} - \nabla_H F_w\right)}^{\text{turbulent-drag force}}$$

✦ Vertical component of vorticity ζ_T

$$\frac{\partial \tilde{\xi}_T}{\partial t} = -\overbrace{\nabla_H \cdot \left(\tilde{\xi}\mathbf{v}\right)_T}^{\text{horizontal advection}} - \overbrace{\left[\frac{\partial}{\partial z}\left(\tilde{\xi} w\right)\right]_T}^{\text{vertical advection}} + \overbrace{\left[\tilde{\boldsymbol{\eta}} \cdot \nabla_H w\right]_T}^{\text{tilting}} + \overbrace{\left[\tilde{\xi}\frac{\partial w}{\partial z}\right]_T}^{\text{stretching}} + \left[w\nabla_H \cdot \left(2\boldsymbol{\Omega}_H\right)\right]_T + \overbrace{\left[\mathbf{k} \cdot \nabla_H \times \mathbf{F}_\mathbf{v}\right]_T}^{\text{turbulent-drag force}}$$

✦ Potential temperature θ

$$\frac{\partial\left(\rho_0\theta\right)}{\partial t} = -\overbrace{\nabla_H \cdot \left(\rho_0\theta\mathbf{v}\right)}^{\text{horizontal advection}} - \overbrace{\frac{\partial}{\partial z}\left(\rho_0\theta w\right)}^{\text{vertical advection}} + \overbrace{\frac{\rho_0 Q}{\Pi}}^{\text{heating}}$$

Anelastic vector vorticity model w equation

- An elliptic equations determines the vertical component of velocity.

- The definition of $\boldsymbol{\eta}$

$$\tilde{\boldsymbol{\eta}} \equiv \boldsymbol{\eta} + 2\boldsymbol{\Omega}_H$$

where $$\boldsymbol{\eta} \equiv \mathbf{k} \times \left(\frac{\partial \mathbf{v}}{\partial z} - \nabla_H w \right)$$

or $$\frac{\partial \mathbf{v}}{\partial z} - \nabla_H w = -\mathbf{k} \times \boldsymbol{\eta}$$

- Continuity equation

$$\nabla_H \cdot \mathbf{v} + \frac{1}{\rho_0} \frac{\partial}{\partial z} \left(\rho_0 w \right) = 0$$

- w equation

$$\nabla_H^2 w + \frac{\partial}{\partial z} \left[\frac{1}{\rho_0} \frac{\partial}{\partial z} \left(\rho_0 w \right) \right] = -\mathbf{k} \cdot \nabla_H \times \boldsymbol{\eta}$$

with $w_T = w_S = 0$

3D poisson equation solver

- Based on Arakawa, Jung and Konor
- The continuous equation

$$\nabla^2 w + \frac{\partial}{\partial z}\left[\frac{1}{\rho}\frac{\partial}{\partial z}(\rho w)\right] = rhs$$

- The discrete equation

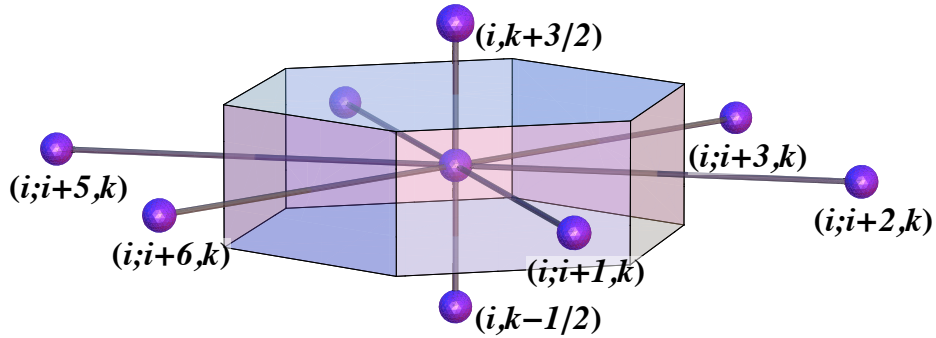

$$\frac{1}{A_i}\sum_{i'}\frac{w^{(\kappa)}_{i+i',k+1/2} - w^{(\kappa+1)}_{i,k+1/2}}{L_{i;i+i'}} l_{i;i+i'}$$

$$+\frac{1}{\delta z_{k+1/2}}\left[\frac{1}{\rho_{k+1}\delta z_{k+1}}\left(\rho_{k+3/2} w^{(\kappa+1)}_{k+3/2} - \rho_{k+1/2} w^{(\kappa+1)}_{k+1/2}\right) - \frac{1}{\rho_k \delta z_k}\left(\rho_{k+1/2} w^{(\kappa+1)}_{k+1/2} - \rho_{k-1/2} w^{(\kappa+1)}_{k-1/2}\right)\right] = rhs_{i,k+1/2}$$

where (κ) denotes an iteration index.

3D poisson equation solver

- Re-arrange to form an implicit tridiagonal system in the vertical

$$\frac{\rho_{k-1/2}}{\delta z_{k+1/2}\rho_k\delta z_k} w_{k-1/2}^{(\kappa+1)} - \left[\frac{1}{A_i}\sum_{i'}\frac{l_{i;i+i'}}{L_{i;i+i'}} + \frac{\rho_{k+1/2}}{\delta z_{k+1/2}}\left(\frac{1}{\rho_{k+1}\delta z_{k+1}} + \frac{1}{\rho_k\delta z_k}\right)\right] w_{i,k+1/2}^{(\kappa+1)} + \frac{\rho_{k+3/2}}{\delta z_{k+1/2}\rho_{k+1}\delta z_{k+1}} w_{k+3/2}^{(\kappa+1)}$$

$$= rhs_{i,k+1/2} - \frac{1}{A_i}\sum_{i'}\frac{l_{i;i+i'}}{L_{i;i+i'}} w_{i+i',k+1/2}^{(\kappa)}$$

- A straightforward modification of the relaxation operator within the 2D multigrid.
- With the current domain decomposition the entire vertical column is local information. Scaling results of the 2D solver will indicate the scaling of the 3D solver.

3D Poisson equation solver: Buoyant bubble test

- Prescribed analytic potential temperature perturbation

$$B = g\frac{\theta'}{\theta_0 (= 300K)}$$

- Implied tendency in the horizontal vorticity equation

$$\frac{\partial \tilde{\boldsymbol{\eta}}}{\partial t} = \ldots - \mathbf{k} \times \nabla_H B$$

- Taking the curl forms the right-hand-side of the w equation.

$$\nabla^2 w + \frac{\partial}{\partial z}\left[\frac{1}{\rho}\frac{\partial}{\partial z}(\rho w)\right] = -\mathbf{k}\cdot\nabla_H \times \boldsymbol{\eta}$$

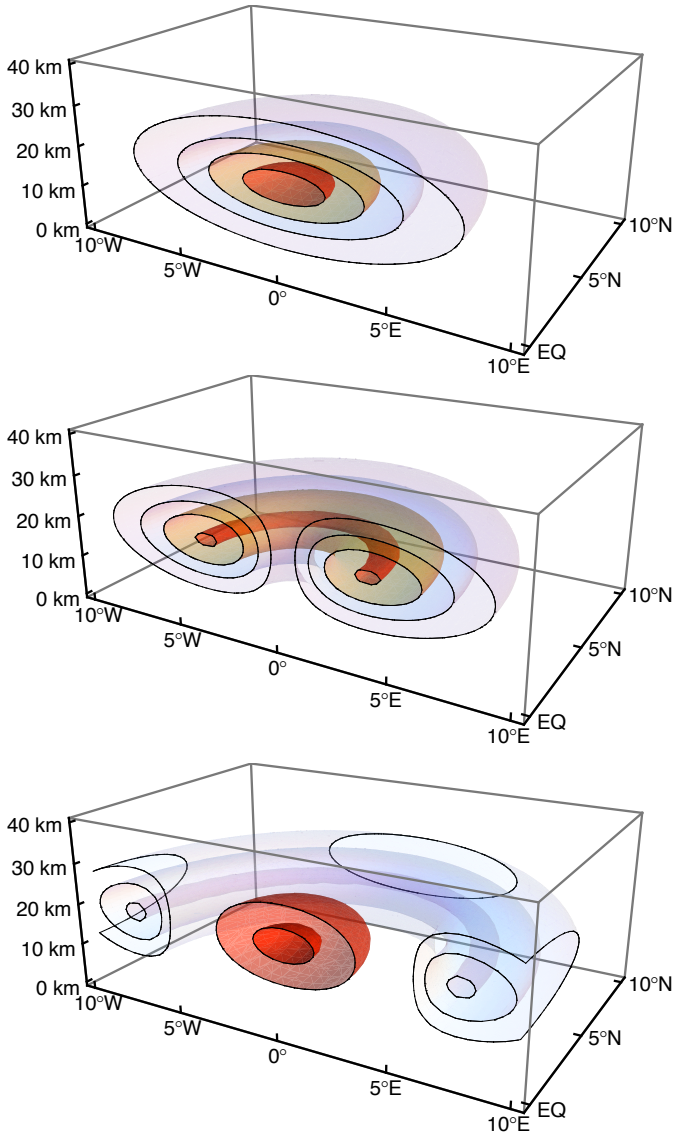

3D Poisson equation solver: Buoyant bubble test

- Plot of grid 6 (resolution 40962 cells)
- Plot shows a cross section through the middle of the bubble

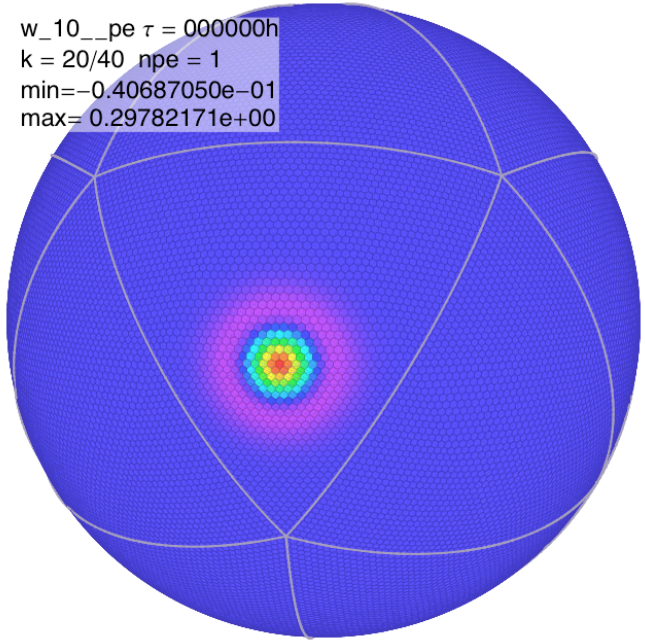

- The convergence properties of grid 7 (resolution 163842 cells)
- The inf-norm of the difference of 2 successive iterations is plotted.

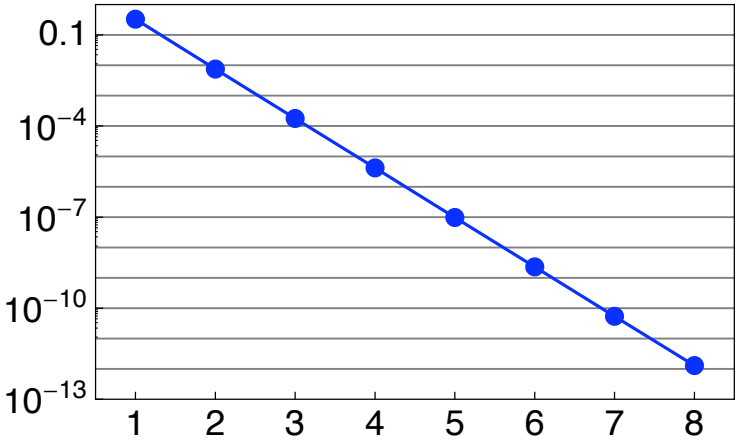

Current status and future work

- Much of the computational infrastructure of the baroclinic model can be reused. e.g. parallel domain decomposition and communication
- Parallel 3D multigrid methods work well for elliptic equations on the icosahedral grid. 2D multigrid scales well to large numbers of processes.
- The stretching and tilting terms in the vorticity equations are straightforward and use many of the grid metrics developed for other operators.
- Advection is defined at cell centers, corners and edges:
  - Centers. 3rd-order upstream biased. Done
  - Corners. 3rd-order upstream biased. Done
  - Edges. Currently being developed.